PHYSICAL REVIEW D **95,** 082004 (2017)

Ground-based low-frequency gravitational-wave detector with multiple outputs

Ayaka Shoda,[1,*] Yuya Kuwahara,[2] Masaki Ando,[1,2,3] Kazunari Eda,[2,3] Kodai Tejima,[2] Yoichi Aso,[1] and Yousuke Itoh[3]

[1]*Gravitational Wave Project Office, Optical and Infrared Astronomy Division, National Astronomical Observatory, Osawa 2-21-1, Mitaka, Tokyo 181-8588, Japan*

[2]*Department of Physics, Graduate School of Science, University of Tokyo, Hongo 3-7-1, Tokyo 113-0033, Japan*

[3]*Research Center for the Early Universe (RESCEU), Graduate School of Science, University of Tokyo, Hongo 3-7-1, Tokyo 113-0033, Japan*

(Received 22 November 2016; published 13 April 2017)

We have developed a new gravitational-wave (GW) detector, TOrsion-Bar Antenna (TOBA), which has a multiple-output configuration. TOBA is a detector with bar-shaped test masses that are rotated by the tidal force of the GWs. In our detector, three independent signals can be derived from the GW by monitoring multiple rotational degrees of freedom, i.e., the horizontal rotations and vertical rotations of the bars. Since the three outputs have different antenna pattern functions, the multioutput system improves the detection rate and the parameter estimation accuracy. This is useful for obtaining further details about the GW sources, such as population and directions. We successfully operated the multioutput detector continuously for more than 24 hours with stable data quality. The GW equivalent strain noise in one of the signals has been reduced to 1×10^{-10} Hz$^{-1/2}$ at 3 Hz by a combination of passive and active vibration isolation systems, while the sensitivities to possible GW signals derived from the vertical rotations are worse than that from the horizontal rotation.

DOI: 10.1103/PhysRevD.95.082004

I. INTRODUCTION

In September 2015, a gravitational wave (GW) was directly detected by the Advanced Laser Interferometer Gravitational-Wave Observatory (aLIGO) for the first time [1]. The detected GW, named GW150914, was the signal from the inspiral and merger of two black holes with masses of about 30 $M_\odot$. The signal was the first evidence of a binary black hole merger. As another event of the black hole merger, GW151226, has since been detected [2], further details of binary black hole systems, such as distribution and population of black holes, might be revealed by further observations.

While aLIGO detected the transients for a few hundred milliseconds, longer observations would provide much better information on the binary systems, such as the spins of the black holes. Binary systems with masses of about 30 $M_\odot$ emit GWs with frequencies of about 0.1 Hz 15 days before the merger. Such a long-term observation of the GW signals from the binary systems would effectively solve the degeneracy of the parameters, such as their spins, which is expected to be a clue about the evolution of black holes [3,4]. In addition to black holes with masses of the order of 10 $M_\odot$, it is important to search for black holes with rather larger and smaller masses. Observation of various black hole mergers would elucidate the evolution process of supermassive black holes. In order to observe the GW signals from binary systems with various masses, it is necessary to observe GWs at various frequencies. Binaries with heavier masses emit GWs at lower frequencies than the observation band of current interferometers.

A TOrsion-Bar Antenna (TOBA) [5] is a GW detector that is sensitive to GWs at around 1 Hz, whereas the observation band of terrestrial interferometric GW detectors, such as LIGO, is above about 10 Hz. One of the astronomical targets of TOBA is intermediate-mass black hole binaries. The space-borne interferometric detectors, such as the Laser Interferometer Space Antenna [6] and the DECI-herz Gravitational-Wave Observatory [7], would also have sensitivity below 10 Hz, but TOBA can be realized on the ground with good access for repair and upgrade, and at a modest cost. Though the final target sensitivity of TOBA is not as good as space detectors, the observation range is expected to be as far as 10 Gpc with the luminosity distance for the intermediate-mass black hole mergers.

TOBA has two bar-shaped test masses that are suspended at their centers. GWs are detected by monitoring their relative rotation excited by the tidal force from GWs. Since the resonant frequencies of the test masses in the torsional modes are as low as a few mHz, TOBA is sensitive to GWs at low frequencies even on the ground. As a proof of concept, the first prototype of TOBA was earlier developed with a single test mass bar [8] and set the upper limits on a stochastic GW background as $\Omega_{\rm gw} h_0^2 < 2 \times 10^{17}$ from 0.035 to 0.830 Hz, where $\Omega_{\rm gw}$ is the GW

*ayaka.shoda@nao.ac.jp

energy density per logarithmic frequency interval in units of the closure density and h0 is the Hubble constant in units of 100 km/s/Mpc [9,10].

The reason for using more than three detectors in order to determine the parameters of binaries, such as masses of the objects, polarization angle, and the sky position of the source is that current individual detectors have poor directivity [11]. Therefore, we proposed the multioutput system, which provides three independent strain signals from a single detector by monitoring multiple rotational degrees of freedom of the test masses [12]. The multioutput system improves the event rate and angular resolution, which would enhance the low-frequency GW astronomy even with fewer detectors.

In this paper, we introduce the first TOBA detector that has the multioutput system: multioutput TOBA. Its main feature is the new suspension system for the multioutput configuration, which also performs as a vibration isolation system. In Sec. II, we explain the principle of the GW detection and the multioutput system, and the target sensitivity. The detector configuration that we developed is described in Sec. III. Its characteristics are mentioned in Sec. IV.

II. TOBA

A. Principle of GW detection using TOBA

TOBA has two bar-shaped test masses that rotate differentially due to the tidal force from GWs as shown in Fig. 1 [5]. The equation of motion of the test mass bar in the rotational mode is

$$I_z\ddot{\theta}(t)+\gamma_z\dot{\theta}(t)+\kappa_z\theta(t)=\frac{1}{4}\ddot{h}_{ij}q_z^{ij}, \tag{1}$$

where θ, I_z, γ_z, and κ_z are the angular fluctuation, the moment of inertia, the damping constant, and the spring constant around the z axis, respectively. h_{ij} is the amplitude of the GW, and q_z^{ij} is the dynamical quadrupole moment of the test mass for rotation along the z axis. The frequency response of the angular fluctuation of the test mass is derived from Eq. (1) as

$$\tilde{\theta}(\omega)=\sum_{A=+,\times}H_A(\omega)\tilde{h}_A, \tag{2}$$

$$H_A(\omega)=\frac{q_A}{2I}\frac{\omega^2}{\omega^2-\omega_0^2(1+i\varphi)+i\omega\gamma_z/I}, \tag{3}$$

where φ and $\tilde{h}_A$ are the loss angle and the amplitude of a GW coming along the z axis with polarizations of $A=+$ and $\times$. $\omega_0=\sqrt{\kappa_z/I}$ is the resonant frequency of the torsional mode, above which the angular fluctuation due to the GW is approximated to be independent of its frequency.

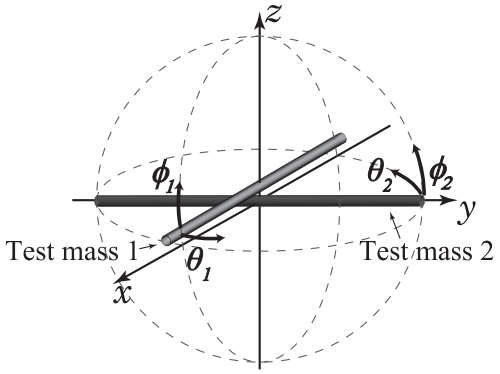

FIG. 1. Schematic view of the TOBA test masses.

In the multioutput system, we also consider rotations of the bars in the vertical planes. Considering the test mass 1 in Fig. 1, the angular fluctuation along the y axis also obeys an equation similar to Eq. (1),

$$I_y\ddot{\phi}_1(t)+\gamma_y\dot{\phi}_1(t)+\kappa_y\phi_1(t)=\frac{1}{4}\ddot{h}_{ij}q_y^{ij}. \tag{4}$$

It means that the bar also rotates in the vertical plane due to GWs coming along the y axis. Therefore, we can derive two independent signals θ and ϕ from the single test mass bar.

Since we have two orthogonal test mass bars, it is possible to derive three independent strain signals from the single detector, i.e., $\theta=\theta_1=-\theta_2$, ϕ_1, and ϕ_2, where the suffix indicates the two test masses. The sensitivity to GW signals derived from θ, $\theta=(\theta_1-\theta_2)/2$, would be better by $\sqrt{2}$ than the sensitivity derived only from one of the rotational signals, when the noise in θ_1, θ_2, ϕ_1, and ϕ_2 is uncorrelated and of similar magnitude. This multioutput system would increase the expected detection rate by about 1.7 times, since the three signals have different sensitive areas in the sky. Also, parameter estimation accuracy for short-duration signals would be improved since the three independent information helps to break the degeneracies of the parameters [12].

B. Target sensitivity and the previous research

The final target sensitivity of TOBA is about 1×10^{-19} $\mathrm{Hz}^{-1/2}$ in strain at 1 Hz as described in [5], which is limited mainly by gravity gradient noise, shot noise, and radiation-pressure noise. The shot noise and the radiation-pressure noise originate from the quantum nature of the laser that is used for the rotation readout system. This sensitivity can be achieved by sensing the rotation of large cryogenic test mass bars with length of 10 m, using a Fabry-Perot interferometer with a wavelength of 1064 nm, a finesse of 10, and an input power of 10 W. The test mass bars and the suspension wires should be cooled down in order to reduce the thermal noise. Since several advanced technologies are

necessary for the final TOBA configuration, it is necessary to develop each component using prototypes.

The first prototype TOBA had been developed previously [8]. It had a single bar-shaped test mass with a magnetic levitation system in order to suspend the test mass softly in the rotational degree of freedom. The test mass had a length of 20 cm, and its horizontal rotation was measured by a Michelson interferometer, which means that it is a single-output configuration. It successfully tested the basic principle of TOBA, and set the first upper limit on the stochastic GW background $\Omega_{\rm gw} < 4.3 \times 10^{17}$ at 0.2 Hz with single detector [9]. The sensitivity of the first prototype TOBA is limited by the magnetic noise induced by the magnetic suspension system, and the seismic noise coupling. The upper limit on the stochastic GW background at the same frequencies has been updated by calculations from the response of the Earth [13] and the Moon [14]. While such measurements are limited by the motion of the planets caused by various perturbations that cannot be decreased, it is possible to update the upper limits further by improving the GW detectors.

As a next step, we have developed a multioutput TOBA, as described in the following sections. Its main purpose is the development of the suspension system that is critical to the multioutput system, and the passive and active vibration isolation systems that attenuate the noise caused by the seismic motion.

III. MULTIOUTPUT TOBA DETECTOR

A. Overview

The schematic view of the multioutput TOBA is shown in Fig. 2. The two orthogonal test masses that sense the GWs are suspended from a hexapod-type active vibration isolation table (AVIT) via an intermediate mass, which is magnetically damped by a damping mass. The optical bench where the sensors and actuators are set is also suspended from the intermediate mass. Except for the actuators and sensors of the AVIT, the entire suspension system is in a vacuum tank.

B. Test masses

A picture of the test masses is shown in Fig. 3. The test masses are designed for the multioutput system and the test of common-mode noise reduction. The two orthogonal test mass bars with the length of 24 cm are suspended by the two parallel wires each, so that the centers of the masses can be located at the same position in order to maximize the common mode noise reduction rate in the horizontal rotation signal. This design was chosen to reduce the noise caused from the common rotational displacements of the bars. The common mode noise reduction rate is expected to be large when the sensitivity is limited by environmental disturbances that effect the test mass rotations in common, while the reduction rate is $\sqrt{2}$ in strain when the noise sources of the two signals are of the same amplitude and independent.

The resonant frequency in the horizontal rotational mode is $f_{\theta 0} = \sqrt{mga^2/Il}/2\pi$, where m, g, a, I, and l are the mass of the test mass, the acceleration of gravity, the distance between the two suspension wires as shown in Fig. 3, the moment of inertia of the test mass, and the length of the wire, respectively. The resonant frequency in the vertical rotational mode is $f_{\phi 0} = \sqrt{mgd/I}/2\pi$, where d is the height distance between the suspension points and the

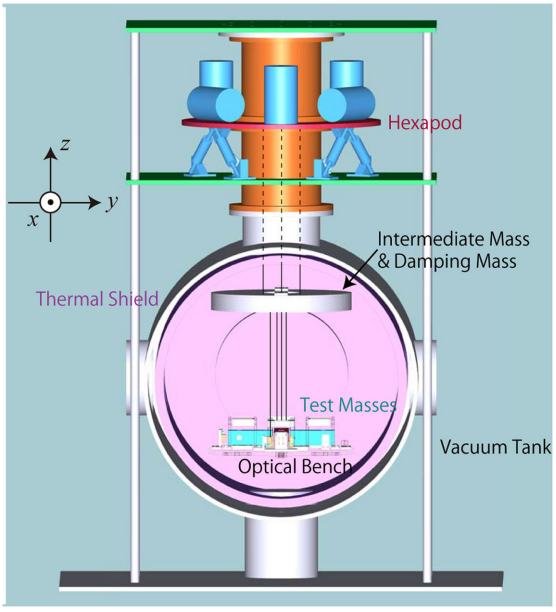

FIG. 2. Overview of the multioutput TOBA.

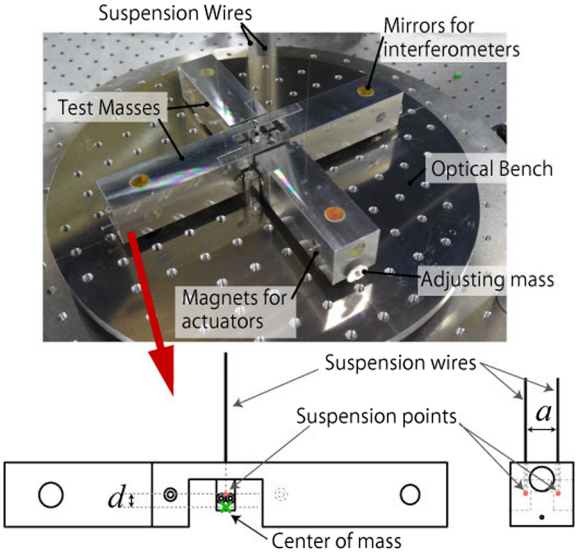

FIG. 3. Picture of the test masses. Each test mass is suspended by two wires so that the center of each mass can be located at the same position.

TABLE I. The main property of the test mass bars and the suspended optical bench.

Test mass	
The length of the bar	240 mm
The mass	0.61 kg
The moment of inertia (horizontal and vertical rotation)	3.34×10^{-3} kg m^2
The quadrupole moment	3.20×10^{-3} kg m^2
The length of the suspension wires	400 mm
The distance between the suspension wires (a)	17 mm
Optical bench	
The mass	4.4 kg
The moment of inertia (horizontal rotation)	6.17×10^{-2} kg m^2
The moment of inertia (vertical rotation)	3.50×10^{-2} kg m^2
The quadrupole moment (vertical rotation)	3.08×10^{-2} kg m^2
The length of the suspension wires	400 mm
The distance between the suspension wires	45 mm

center of mass as shown in Fig. 3. The suspension points of the test masses are set to be close to their center of mass in order to minimize the resonant frequency of the vertical rotation. The parameters in our setup are summarized in Table I. From these parameters, the resonant frequencies of the bars in the horizontal and vertical rotation are derived to be 0.10 and 0.15 Hz, respectively. The resonant frequencies are set at around 100 mHz in our prototype in order to realize the new suspension system with the compact setup. The resonant frequencies would be pushed down by using larger test masses in the future upgrade in order to widen the observation band.

C. Readout system

The main sensors that we used in the multioutput TOBA are Michelson interferometers. The motion of the bar is monitored by measuring the phase shift of the beam reflected by the mirrors attached at the bar. Since it is necessary to have several sensors around the test masses in order to monitor three independent rotational signals, fiber optics are used for space saving. The sensor configuration is shown in Fig. 4. The type-1 interferometers, which measure the displacement of each mirror attached on the test masses, monitor the yaw, longitudinal, and side motion of the bar. The type-2 interferometers that sense the differential displacement of the two end mirrors are used as sensors for the roll motion. The position of the test masses is controlled by the coil-magnet actuators so that each interferometer can be kept at its working point. The GW signals are derived from the feedback signal on the actuators. The test masses are controlled in their longitudinal, side, yaw, and roll modes. These sensors are mounted on the suspended optical table explained in the next subsection.

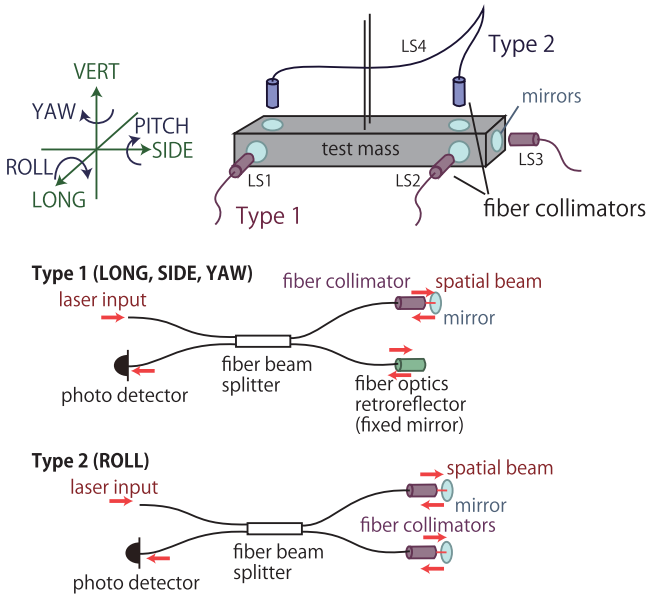

FIG. 4. Configuration of the fiber laser interferometers.

D. Vibration isolation system

Though the seismic motion in the rotational degree of freedom is small, a seismic vibration isolation system is necessary since translational vibration couples to the rotational signals. For example, nonparallel mirrors at both ends of the test mass induce translational seismic noise coupling [15,16]. The test masses, and the optical table where the sensors and actuators are set, are suspended in order to attenuate the seismic motion above the resonant frequencies of those pendulum modes. However, since the resonant frequencies of the pendulum modes are about 1 Hz, an additional seismic isolation system for low frequencies is necessary for TOBA. Therefore, we developed an AVIT for low-frequency vibration isolation and the whole system is suspended from the AVIT.

The AVIT is a table with six legs composed of piezoelastic elements (PZTs) as shown in Fig. 5. The PZTs

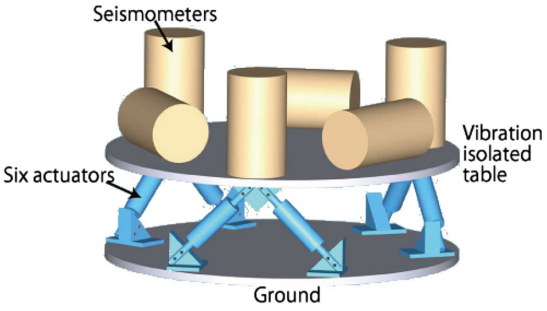

FIG. 5. Schematic view of the Hexapod-type AVIT. The whole suspension system is suspended from the top table. It has six piezoelastric actuators as legs so that they can actuate the top table in six degrees of freedom. The six seismometers are attached in order to sense the vibration of the top table.

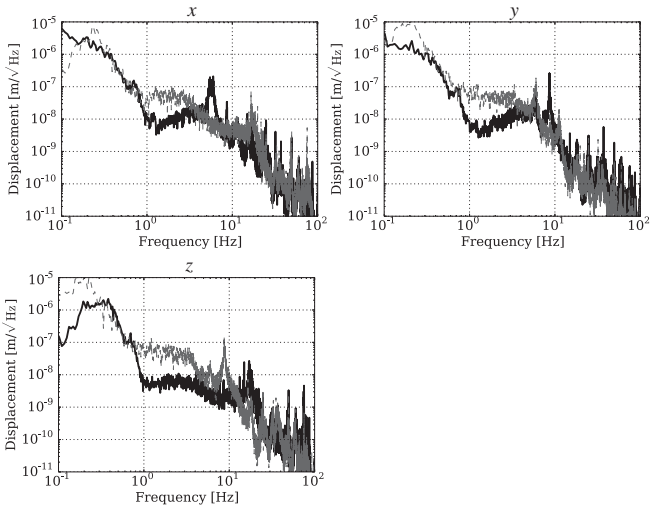

FIG. 6. Seismic isolation performance of the AVIT in each linear degree of freedom. The dashed lines represent the seismic displacement with the AVIT off, and the solid lines represent one with the AVIT on. The coordinates are defined in Fig. 2.

(P844.30, products of Physik Instrumente) move the top plate. They have tips with slits at both ends in order to avoid nonlinear effects when they push or pull the table. The vibration of the top table is suppressed by feedback control using six seismometers (L-4C geophones, products of Sercel) mounted on the top plate and the PZTs. Note that reflective position sensors are used to measure the position of the top table relative to the ground at very low frequencies since the lack of sensitivity of seismometers at low frequencies causes drift of the top table.

The seismic displacement of the top table is shown in Fig. 6. The vibration isolation ratio from the ground motion at 1 Hz achieved is almost ten times. Its performance is mainly limited by the range of the PZTs and the resonance of the frame where the AVIT is sitting.

The AVIT can attenuate the vibration at around 1 Hz even with its compact body 45 cm in diameter, while passive vibration isolation requires a large mechanism for low-frequency vibration isolation, such as inverted pendulums [17–19]. Also the AVIT can effectively attenuate the vibration of the heat link in the cryogenic system for thermal noise reduction that is planned to be implemented in the future upgrade. This is because the rigid structure enables the AVIT to suppress the vibration induced directly into the vibration attenuated plate, i.e., the vibration of the heat link attached at the suspension point.

IV. DETECTOR CHARACTERIZATION

A. Calibration

The feedback signal of the control system is converted to the relative angular fluctuation using the transfer functions of the control system. The transfer functions are directly measured by injecting signals into the control loop. The signals of angular fluctuation are converted to GW amplitude equivalent signals using theoretical calculations since it is difficult to produce a large tidal force that affects the detector similarly as GWs. And the transfer function depends on the mechanical property of the detector. In this section, the transfer function from the angular fluctuations to GW amplitudes is calculated.

The angular fluctuations of the test masses are read by the laser interferometers. The angles are calibrated into the GW signal outputs as follows:

$$s_1 = \frac{1}{H_{\times 1}}\frac{1}{2}(\theta_1 - \theta_2), \tag{5}$$

$$s_2 = \frac{1}{H_{\times 2}}\phi_1, \tag{6}$$

$$s_3 = \frac{1}{H_{\times 3}}\phi_2, \tag{7}$$

where $H_{\times i}$ $(i = 1, 2, 3)$ are defined as

$$H_{\times i} = H_{\times i}^{\mathrm{TM}} - H_{\times i}^{\mathrm{OB}}; \tag{8}$$

$H_{\times i}^{\mathrm{TM}}$ and $H_{\times i}^{\mathrm{OB}}$ are the transfer functions from the GW signal to the angular fluctuations of the test masses and the optical bench derived from Eq. (3), respectively. Here, H_{+i} are considered to be 0's since $q_+ = 0$ when the test masses are suspended along the x axis and y axis. It is necessary to take $H_{\times i}^{\mathrm{OB}}$ into account since what we measure is relative motion between the optical bench and the test masses. $H_{\times i}^{\mathrm{OB}}$ is not negligible since the optical bench is also sensitive to GWs due to the suspension system.

In our case, the H_{Ai}^{TM} are

$$H_{\times i}^{\mathrm{TM}} \simeq \frac{q_{\times i}^{\mathrm{TM}}}{2I_i^{\mathrm{TM}}} = 0.48 \tag{9}$$

above their resonant frequencies, where $i = 1$, 2, and 3. For the optical bench,

$$H_{\times 1}^{\mathrm{OB}} \simeq 0, \tag{10}$$

$$H_{\times 2,3}^{\mathrm{OB}} \simeq \frac{q_{\times 2,3}^{\mathrm{OB}}}{2I_{2,3}^{\mathrm{TM}}} = 0.44. \tag{11}$$

$H_{\times 2,3}^{\mathrm{OB}}$ are not 0 because the side view of the optical bench does not show four-fold symmetry, while $H_{\times 1}^{\mathrm{OB}}$ is derived to be 0's from $q_{\times 1}^{\mathrm{OB}} = 0$. Therefore, the calibration factors for the s_2 and s_3 are about ten times smaller than s_1 in our setup as shown in Figs. 7 and 8 above 2 Hz.

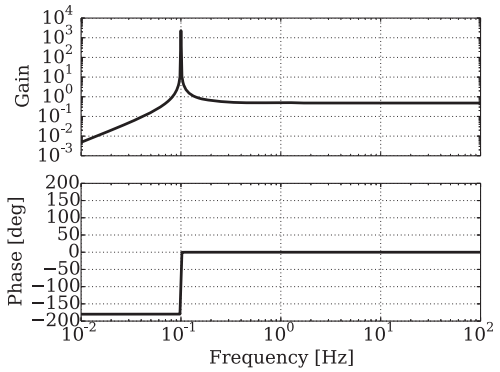

FIG. 7. Calibration factor from the horizontal rotational angle to s_1, which is the GW amplitude equivalent signal derived from the horizontal rotation of the bars. Above the resonant frequency of the horizontal rotation at 0.1 Hz, the calibration factor is constant as derived from Eq. (3).

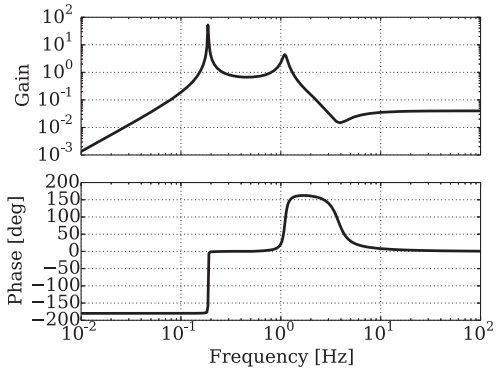

FIG. 8. Calibration factors from the vertical rotational angle to $s_{2,3}$, which are the GW amplitude equivalent signals derived from the vertical rotation of each bar. The peak at 0.15 Hz is the resonant frequency of the vertical rotation of the bar. Above the resonant frequency of the optical bench, which is 1.1 Hz with the quality factor of 10, the calibration factor is decreased because the optical bench also rotates due to the GW.

B. Sensitivity and noise sources

The solid lines in Fig. 9 are the GW strain equivalent noise spectra obtained from the multioutput TOBA. The dotted line is the sensitivity of the first prototype. It shows that the sensitivity of s_1 (represented by the black line in Fig. 9) is improved by up to about 100 times compared to the first prototype. Figure 10 shows the dominant noise sources in the three signals. The sensitivity of the multi-output TOBA is limited mainly by the interferometer readout noise and the seismic coupling noise. The readout noise, shown by the solid dark gray lines, is estimated from the readout signal measured with the test masses fixed on the optical bench. It is thought to be induced by the fiber optics since the contribution from the other laser noise sources, such as the intensity fluctuation and the frequency fluctuation, are lower than the measured readout noise.

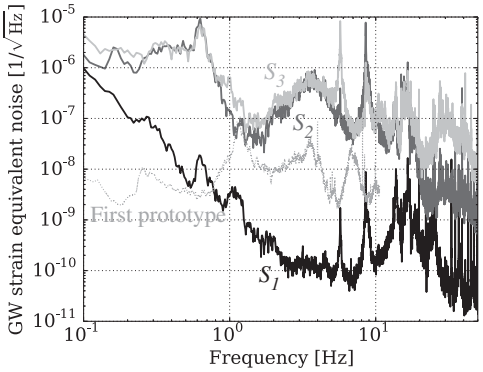

FIG. 9. GW equivalent noise spectra obtained from the multi-output TOBA compared with the spectrum of the previous detector. The black, dark gray, and light gray lines are the spectra of s_1, s_2, and s_3, respectively. The dotted gray line represents the sensitivity of the previous detector [9].

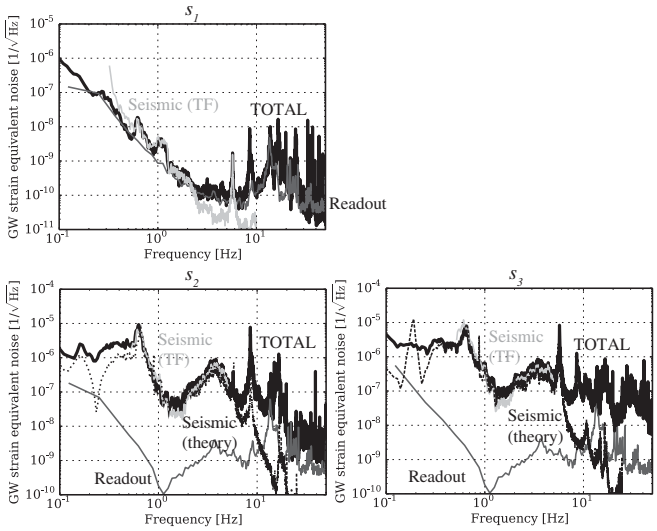

FIG. 10. GW equivalent noise spectra and the spectra of the respective noise sources. The top left, bottom left, and bottom right graphs are the sensitivities and the noise sources of s_1, s_2, and s_3, respectively. The black lines are the GW equivalent noise spectra. The dark gray lines show the readout noise measured with the test mass fixed to the optical bench. The light gray lines are the seismic noise estimated from the transfer function from the ground to the sensor directly measured using the AVIT. The dotted dark gray lines are the seismic noise calculated using the theoretical transfer function from the ground to the sensor. The theoretically calculated seismic noise is not plotted in the left top, since the coupling mechanism of seismic noise to s_1 is unknown.

The mechanical vibration of the fibers is considered to appear as phase noise at higher frequencies than 8 Hz because of the many peaks. What causes the phase noise at lower frequencies is under investigation. The light gray lines are the seismic noise estimated from the motion of the AVIT measured by the seismometers on the AVIT and the transfer functions from the seismometers to the laser

sensors directly measured by exciting the AVIT. While the coupling mechanism to s_1 is now under investigation, the seismic noises of s_2 and s_3 are induced because the translational seismic motions excite the vertical rotations of the test masses. Since the heights of the suspension point and of the center of mass are different, the translational force on the suspension point applies a torque in the roll direction. The dotted dark gray lines in the two bottom spectra in Fig. 10 are the seismic noise calculated from the theoretical transfer functions from the ground to the test masses. The sensitivity curve, the seismic noise estimated from the measured transfer functions, and the theoretical seismic noise fit well for s_2 and s_3. In addition to the large seismic coupling, the small calibration factor from the rotation to the GW amplitude, as derived in the previous section, makes the sensitivity of s_2 and s_3 about 1,000 times worse than s_1.

The performance of the common mode noise rejection between the two test masses is shown in Fig. 11. As described in Sec. III B, the centers of masses are designed to be at the same position since the noise is expected to be reduced when the sensitivity is limited by the common rotational displacement. However, subtraction of the two signals is not effective for the noise reduction in our case, since there is almost no coherence between them. The readout noise is not correlated between the two independent interferometers. Also the seismic coupling noise is not correlated, since the seismic motion in the y direction couples to the rotation signal of the test mass 2, and the motion in the x direction couples to the signal of the test mass 1 in Fig. 1. Since there is no correlation between the seismic motions in the orthogonal directions, the two rotational signals are also not correlated.

Figure 12 shows the effectiveness of the AVIT. The dotted gray lines are the sensitivity measured without vibration attenuation using the AVIT, while solid black lines are the sensitivity measured with the AVIT working.

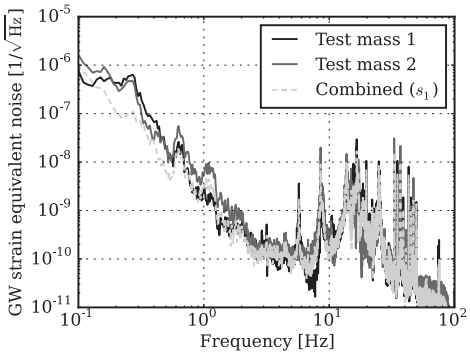

FIG. 11. Effect of the common mode noise rejection. The black and the dark gray lines are the strain sensitivities calculated using single test mass, 1 and 2, respectively. The dotted light gray line is the sensitivity derived by subtraction of the signals from the two test masses.

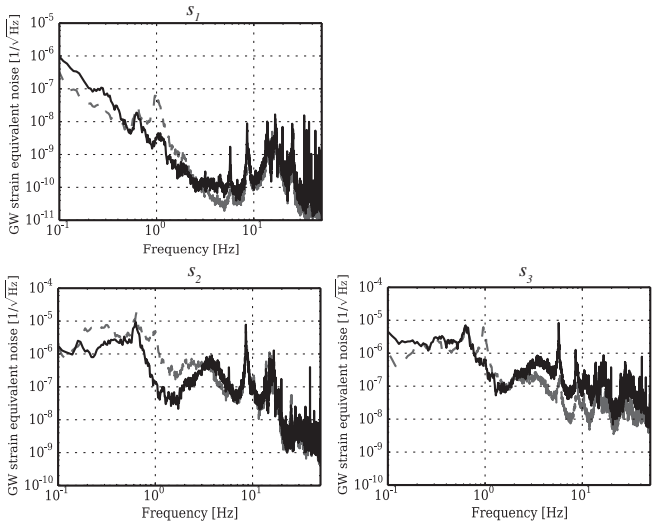

FIG. 12. Sensitivities of signals with the AVIT on and off. The top, bottom left, and bottom right graphs represent the sensitivity of s_1, s_2, and s_3, respectively. The black lines are the sensitivities with the AVIT on, while the dashed gray lines are the ones with AVIT off.

The sensitivity at around 1 Hz improved by a large amount thanks to the AVIT. At 4–10 Hz, the noise levels are made worse by the AVIT. It is thought to be the control noise induced by the AVIT since the resonance of the support frame disturbs the AVIT control loops too much to allow enough phase margin.

C. Stability and Gaussianity

We performed the observational run from 10:50 UTC, December 10, 2014 to 10:50 UTC, December 11, 2014. The observation system operated stably for more than 24 hours.

The spectrograms of the three signals during the observation are shown in Fig. 13. The noise levels are almost the same though 24 hours except during the earthquake, which occurred at around 20:00, December 10.

The time series data were divided with the segments of 200-sec length with overlap of 50% and converted to square root of the power spectrum density. Defining the frequency domain data at kth frequency f_k in the jth segment for each signal s_i ($i = 1, 2$, and 3) as $s_i^j(f_k)$, we can calculate histograms of $s_i^j(f_k)/\langle s_i(f_k)\rangle$, where $\langle s_i(f_k)\rangle$ is the average over all segments, as shown in Fig. 14. The columns represent the signals, s_1, s_2, and s_3, and the lines represent the frequencies of the collected data, 1, 2, and 8 Hz, respectively. All three signals have Gaussian distributions.

Using these data, we performed several GW search analyses: for continuous GWs, stochastic GW backgrounds, and intermediate mass black hole binaries. Continuous GW signals have been searched for at 6–7 Hz and set an upper limit of 3.6×10^{-12} on the

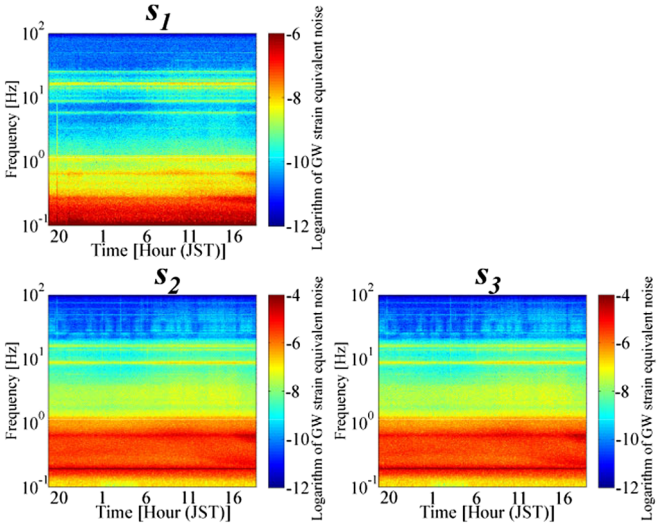

FIG. 13. Spectrograms of the power density of the three signals during the 24-hour observation from 0.1 to 100 Hz.

dimensionless GW strain at 6.84 Hz [20]. Also, at 2.58 Hz, a new upper limit $\Omega_{\rm gw}h_0^2 < 6.0 \times 10^{18}$ was set on the energy of the stochastic GW background [21], while the upper limit set by the first prototype was $\Omega_{\rm gw}h_0^2 < 2 \times 10^{17}$ at 0.035–0.830 Hz. The value of the upper limit was not as good as the first prototype because the upper limit was set at higher frequency than that of the first prototype. It is difficult to set the better upper limit at higher frequencies since the relation between $\Omega_{\rm gw}(f)$ and an observed GW strain amplitude $s(f)$ is $\Omega_{\rm gw}(f) \propto f^3|s(f)|^2$. The GWs from the binary systems with mass of 100 $M_\odot$, and 200–1000 $M_\odot$, were searched using the matched filtering method, and no signals had been discovered [16,22]. The continuous GW signals and GWs from the binary systems were searched at around 1–10 Hz for the first time. The upper limit on the energy of the stochastic GW background has also been approved using the detector with improved sensitivity.

V. DISCUSSION AND FUTURE PLAN

The sensitivity of TOBA was improved mainly by the passive and active vibration isolation systems. The pendulum suspension system provides passive vibration isolation to reduce the seismic motion above 1 Hz. The vibration isolation system for the sensors, as well as for the test masses, is effective. In addition, the AVIT was introduced to reduce the seismic motion around 1 Hz. While its performance was limited by the resonance of the frame where the AVIT is sitting and by the actuation range of the PZTs, the seismic motion of the table is reduced by about

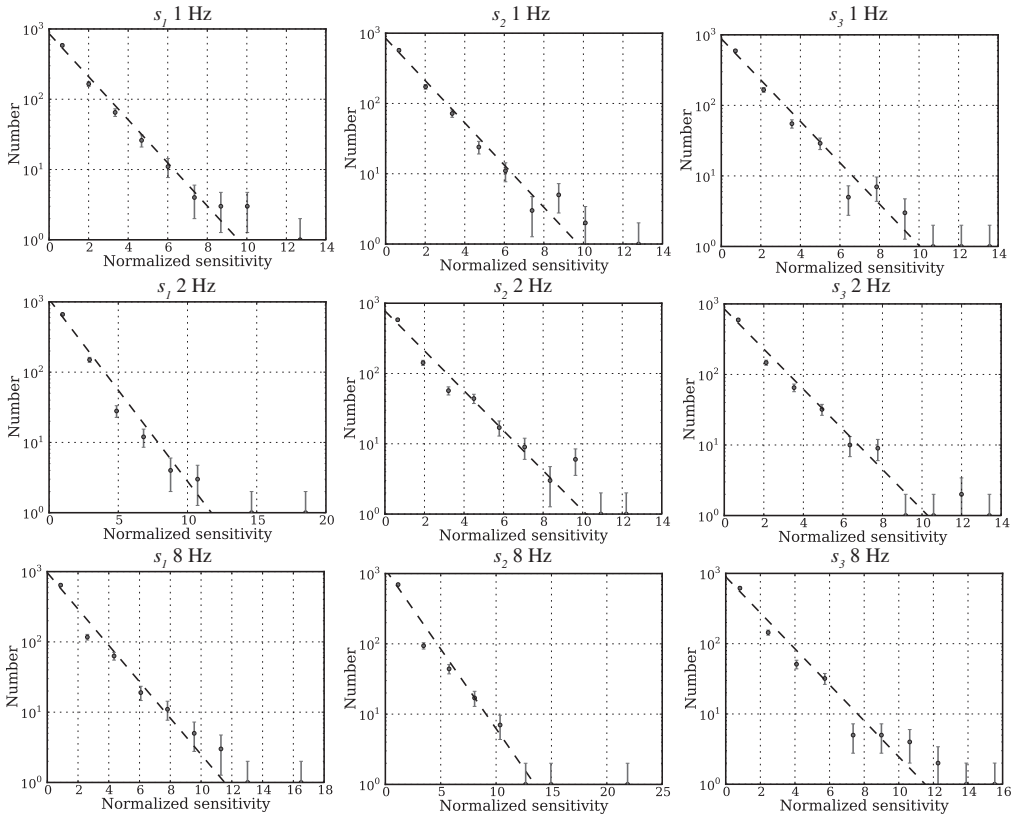

FIG. 14. Histograms of the normalized power spectral density of s_1, s_2, and s_3 at 1, 2, and 8 Hz. The dotted line at each panel corresponds to a Gaussian distribution.

ten times relative to the ground in the three translational degrees of freedom. The combination of that vibration isolation system improves the sensitivity at around 1–10 Hz by 10–100 times compared with the previous prototype TOBA.

Also, the three independent signals are successfully obtained simultaneously and stably, although the sensitivity of the signals from the vertical rotational motion is worse than that from the horizontal rotational motion. The sensitivity was different among the three signals because of the large coupling from the seismic motion and the cancellation of the GW signals between the test masses and the optical bench.

In order to further improve the detector performance with similar setup, careful optimization of the suspension design is necessary. Reinforcement of the frame for the AVIT is required to gain more vibration attenuation ratio, since the large resonances of the base of the AVIT limit its performance. The control gain should be achieved, and the controlled frequency band should be pushed up by using the more solid base for the AVIT. The shape of the optical bench should have four-fold symmetry in order to improve the sensitivities of s_2 and s_3 so that the optical bench does not react to GWs. Also, the positions of the centers of masses of the test masses and the optical bench should be adjusted from the outside of the vacuum tank using moving masses and actuators, such as picomotors, in order to search for the state that minimizes the seismic coupling. Such a modification would also help to investigate the seismic coupling mechanism in the torsion pendulum further. In addition to the suspension design, the readout system needs to be modified in order to improve the sensitivity. Having more space on the optical bench would enable us to use spatial laser beams instead of the fiber optics.

For yet further sensitivity improvement, it is necessary to upgrade several technologies. Other than the seismic attenuation system developed in this work, a low-loss suspension system and a cryogenic system are critical to achieve the final target sensitivity. Also, the configuration for the multioutput system needs to be investigated further, even though the demonstration with our detector was successful. For example, reduction of the suspension thermal noise in the vertical rotational signals is important. Also, it is necessary for the two vertical rotation signals to improve the detector configuration by the methods as explained in the previous section in order to achieve the same sensitivities as the horizontal rotation signal. However, since the fundamental noise sources for the vertical rotation are the same as the ones for the horizontal rotation, the achievable sensitivities of s_2 and s_3 are expected to be almost same as s_1.

For the midterm upgrade that would take about 5 years, GW strain equivalent noise of 10^{-15} at 0.1 Hz. Besides further optimization for the seismic coupling reduction, the key technology for the midterm upgrade would be low-loss suspension for the reduction of the thermal noise. The target sensitivity in this phase is such that the gravity gradient effect, so-called Newtonian noise, could be observed. The gravity gradient effect is the noise caused by the gravity perturbation due to the seismic motion, acoustic sound, motion of the object around the detector, and so on [23]. It is necessary to develop a method for Newtonian noise cancellation for the further sensitivity improvement below 1 Hz. Conversely, precise detection of gravity gradient signals caused by earthquakes would also be applicable to providing early alerts of large earthquakes. The gravity gradient signal from a large earthquake is under consideration as a prompt alert of earthquakes since the gravity signal propagates at the speed of light, which is much faster than the seismic waves [24]. The full-tensor configuration realized by the multioutput system would also be effective for the gravity gradient detection and cancellation [25].

It is expected to take another a few decades to achieve the final target sensitivity, 1×10^{-19} $\mathrm{Hz}^{-1/2}$. The rotation of the test mass with the length of 10 m has to be read by the Fabry-Perot interferometer in order to reduce the shot noise. Also, a cryogenic system to reduce the thermal noise is critical in order to improve the sensitivity at low frequencies. With this sensitivity, intermediate-mass black holes binaries at the luminosity distance of 10 Gpc would be observed with the signal to noise ratio of 5 [5]. Such observational results would be a key to reveal the evolution processes of stellar and supermassive black holes, globular clusters, and galaxies.

VI. SUMMARY

We have developed a new TOBA detector, which employs a new suspension system for the multioutput system. It successfully worked as a multioutput detector, i.e., the three independent signals were derived simultaneously from the single detector. It demonstrates a new technique to improve the event rate and the parameter estimation accuracy. Also, the sensitivity obtained from the horizontal rotational signal is improved from the previous prototype because of the passive and active vibration systems. The AVIT, which is the compact active vibration isolation system realized with the PZT actuators and seismometers, reduced the seismic displacement at lower frequencies than the resonant frequency of the pendulum. The AVIT is also expected to be effective for the vibration isolation for the heat link for the cryogenic system that is planned to be used in the future. Those new technologies would be a new step towards low-frequency GW astronomy. While it is necessary to develop other technologies, such as a cryogenic system and a large system, observation of the binary black hole systems with multioutput TOBA would provide various astronomical information.

ACKNOWLEDGMENTS

This work is supported by Grants-in-Aid from the Japan Society for the Promotion of Science (JSPS), JSPS Fellows Grants No. 26.8636 (K. E.), No. 24.7531, and No. 15J11064 (A. S.). This work is also supported by JSPS Grants-in-Aid for Scientific Research (KAKENHI) Grants No. 24244031 (M. A.), No. 24103005, No. 15H02082, and No. 15K05070 (Y. I.).

[1] B. P. Abbott *et al.*, Phys. Rev. Lett. **116**, 061102 (2016).
[2] B. P. Abbott *et al.*, Phys. Rev. Lett. **116**, 241103 (2016).
[3] B. P. Abbott *et al.*, Astrophys. J. **818**, L22 (2016).
[4] T. Nakamura, M. Ando, T. Kinugawa, H. Nakano, K. Eda, S. Sato, M. Musha, T. Akutsu, T. Tanaka, N. Seto *et al.*, Prog. Theor. Exp. Phys. (**2016**) 093E01.
[5] M. Ando, K. Ishidoshiro, K. Yamamoto, K. Yagi, W. Kokuyama, K. Tsubono, and A. Takamori, Phys. Rev. Lett. **105**, 161101 (2010).
[6] S. Vitale, Gen. Relativ. Gravit. **46**, 1730 (2014).
[7] S. Kawamura *et al.*, Classical Quantum Gravity **28**, 094011 (2011).
[8] K. Ishidoshiro, M. Ando, A. Takamori, K. Okada, and K. Tsubono, Physica (Amsterdam) **470C**, 1841 (2010).
[9] K. Ishidoshiro, M. Ando, A. Takamori, H. Takahashi, K. Okada, N. Matsumoto, W. Kokuyama, N. Kanda, Y. Aso, and K. Tsubono, Phys. Rev. Lett. **106**, 161101 (2011).
[10] A. Shoda, M. Ando, K. Ishidoshiro, K. Okada, W. Kokuyama, Y. Aso, and K. Tsubono, Phys. Rev. D **89**, 027101 (2014).
[11] B. F. Schutz, Classical Quantum Gravity **28**, 125023 (2011).
[12] K. Eda, A. Shoda, Y. Itoh, and M. Ando, Phys. Rev. D **90**, 064039 (2014).
[13] M. Coughlin and J. Harms, Phys. Rev. Lett. **112**, 101102 (2014).
[14] M. Coughlin and J. Harms, Phys. Rev. D **90**, 102001 (2014).
[15] K. Ishidoshiro, Ph.D. thesis, University of Tokyo, 2010.
[16] A. Shoda, Ph.D. thesis, University of Tokyo, 2015.
[17] A. Takamori, P. Raffai, S. Márka, R. DeSalvo, V. Sannibale, H. Tariq, A. Bertolini, G. Cella, N. Viboud, K. Numata *et al.*, Nucl. Instrum. Methods Phys. Res., Sect. A **582**, 683 (2007).
[18] F. Matichard *et al.*, Precis. Eng. **40**, 273 (2015).
[19] S. Braccini, C. Bradaschia, M. Cobal, R. Del Fabbro, A. Di Virgilio, R. Flaminio, A. Giazotto, H. Kautzky, M. Morganti, D. Passuello, E. Calloni, L. Di Fiore, L. E. Holloway, and V. Montelatici, Rev. Sci. Instrum. **64**, 310 (1993).
[20] K. Eda, A. Shoda, Y. Kuwahara, Y. Itoh, and M. Ando, Prog. Theor. Exp. Phys. (**2016**), 011F01.
[21] Y. Kuwahara, A. Shoda, K. Eda, and M. Ando, Phys. Rev. D **94**, 042003 (2016).
[22] R. Sato, T. Morozumi, Y. Michimura, A. Shoda, and M. Ando (to be published).
[23] P. Saulson, Phys. Rev. D **30**, 732 (1984).
[24] J. Harms, J.-P. Ampuero, M. Barsuglia, E. Chassande-Mottin, J.-P. Montagner, S. N. Somala, and B. F. Whiting, Geophys. J. Int. **201**, 1416 (2015).
[25] J. Harms and H. J. Paik, Phys. Rev. D **92**, 022001 (2015).